

Magneto-optical response of InAs lens-shaped self-assembled quantum dots

Seungwon Lee, Fabiano Oyafuso, Paul von Allmen, and Gerhard Klimeck
Jet Propulsion Laboratory, California Institute of Technology, Pasadena, California 91109
(Dated: May 20, 2003)

The magneto-optical response of electron and hole levels for InAs lens-shaped self-assembled quantum dots is investigated with an $sp^3d^5s^*$ nearest-neighbor empirical tight-binding model. Electron and hole energies and the absorption rates of electron-hole pairs are calculated as functions of magnetic field. The Zeeman splitting of electron levels scales linearly with magnetic field, yielding g-factors ranging from 2.0 to 3.5. In contrast, the Zeeman splitting of hole levels demonstrates a nonlinear dependence on the magnetic field. This nonlinearity is due to the strong coupling between closely-spaced hole levels. Calculated absorption spectra demonstrate the existence of strong selection rules for electron-hole pair creation in the self-assembled dots. The selective dipole coupling between electron and hole levels remains intact even at a high magnetic field.

Various conventional and quantum devices using spin carriers in semiconductor quantum dots have been proposed recently.¹⁻³ These applications utilize spin-related phenomena in quantum dots such as Zeeman splitting, exchange interaction, spin blockade, and Kondo effects. The successful realization of these applications relies on the understanding of fundamental spin properties such as effective g-factors, exchange coupling strengths, etc. These spin properties are directly related to the electronic structure of quantum dots. In this work, we demonstrate a realistic modeling of the electronic structure for InAs self-assembled quantum dots and investigate the magneto-optical response, i.e., Zeeman splitting and transition rates between electron and hole levels.

A self-assembled dot is a strongly strained system and hence the accurate modeling of a strain profile is an essential prerequisite for electronic-structure calculations. We apply an atomistic elasticity model to calculate the strain profile of an InAs self-assembled dot embedded in a GaAs buffer layer.^{4,5} The thickness of the buffer layer needed for the electronic structure to converge is found to be as big as the dimension of the dot.⁶ Therefore, we model a strained system consisting of an InAs lens-shaped dot with diameter 10 nm and height 2 nm and a GaAs buffer layer with thickness 10 nm in each direction. The dot is composed of 26392 atoms and the buffer layer of 19688 atoms.

The electronic structure of the strained InAs dot is modeled in the framework of an $sp^3d^5s^*$ nearest-neighbor empirical tight-binding model. Each atom is described by 20 tight-binding basis states (10 orbitals \times 2 spin states). The atomic energies of tight-binding basis states and the coupling between basis states on nearest-neighbor atoms are obtained by fitting them to bulk band structures with a genetic algorithm.^{6,7} To take into account the effect of the displacements of atoms from unstrained crystal structures, the atomic energies are adjusted by a linear correction within the Löwdin orthogonalization procedure.^{7,8} The coupling parameters between nearest-neighbor orbitals are also modified according to the generalized version of Harrison's d^{-2} scaling law and Slater-Koster direction-cosine rules.^{9,10}

We incorporate the spin-orbit and the vector poten-

tial coupling directly into the tight-binding Hamiltonian instead of treating them as a perturbation. Spin-orbit coupling is limited to the same atomic site interaction since the coupling scales as $1/R^3$ with distance R between orbitals.¹¹ The vector potential is incorporated into the Hamiltonian by invoking the Peierls substitution.¹² This substitution approximates the vector potential and its spatial derivatives as same-site, same-orbital interactions.¹³ The final equation derived from this approach is gauge invariant and does not introduce any extra adjustable parameters.^{13,14}

We use the implicitly restarted Arnoldi method to obtain the eigenvalues and eigenvectors of the tight-binding Hamiltonian.¹⁵ This method is most appropriate for large sparse N by N matrices where a matrix-vector product requires order N rather than order N^2 floating point operations. We choose this method because the tight-binding Hamiltonian is a sparse matrix due to the short-ranged coupling between basis states and the size of the Hamiltonian is large ($921600 = 46080 \text{ atoms} \times 20 \text{ basis states}$). Computation is conducted on a Beowulf cluster which consists of 30 nodes linked by a 100 Mb/s ethernet adaptor. Each node is composed of dual Pentium III 800 MHz processors and 2 GB RAM. The wall-clock computation time required to obtain 10 eigenvalues and eigenvectors with 10^{-8} eV accuracy and on 20 processors in parallel is about 6 hours.

The single-particle levels of InAs self-assembled dots are calculated as a function of magnetic field. Figures 1 and 2 show the evolution of the conduction and valence electron energies, as magnetic field B increases from 0 T to 18 T. The direction of the magnetic field is along the growth direction of the self-assembled dot. The magnetic field leads to level splittings. The level splitting is smaller than the confinement energies which are roughly the level spacings at a zero magnetic field. Therefore, we can explain the level splitting in terms of the first-order correction of the Zeeman interaction $((L_z + 2S_z)\mu_B B)$, where L_z and S_z are the z -component of the angular momentum and spin, respectively. μ_B is the Bohr magneton.

The lowest conduction electron level splits into spin up/down levels in the presence of a magnetic field. The

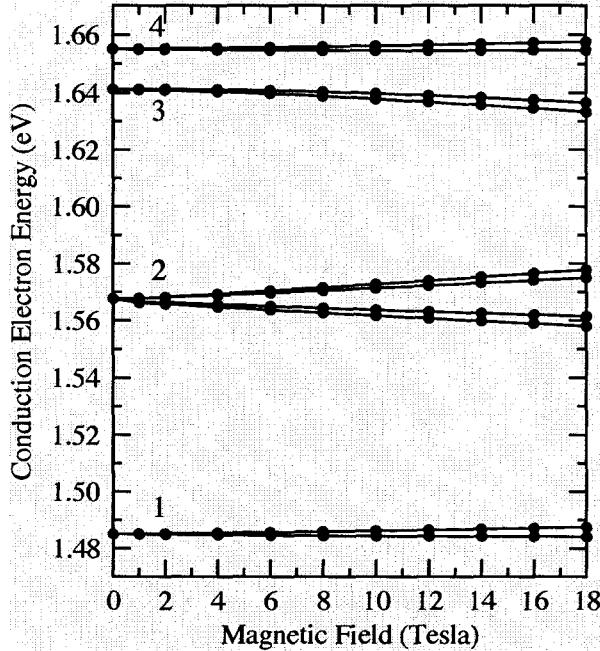


FIG. 1: Conduction electron energies versus magnetic field along the growth direction of InAs self-assembled quantum dots. The lowest conduction electron level splits into two levels due to the s-like symmetry of its envelope function and a lifted spin degeneracy, while the second lowest electron level splits into four levels due to the p-like symmetry of its envelope function and a lifted spin degeneracy. The Zeeman splitting between the spin up and down levels scales linearly with magnetic field, yielding g-factor ranging from 2.0 to 3.5. The number near each line is the index for the conduction level from the lowest.

second lowest level splits into four levels where the upper two levels are the spin up/down states with $L_z = 1$, and the lower two levels are the spin up/down states with $L_z = -1$. The third and fourth conduction levels also split into two levels due to a lifted spin degeneracy. The Zeeman splitting ($E_\uparrow - E_\downarrow$) of the spin up and down energies for all the four conduction levels scales linearly with magnetic field. The effective g-factor defined as $g = (E_\uparrow - E_\downarrow)/\mu_B B$ ranges from 2.0 to 3.5.

The effect of magnetic field on the valence levels is complicated due to the coupling between closely-spaced valence levels. The highest valence level splits into spin up and down levels. The second and third highest valence levels also split into spin up and down levels. The spin down component of the second valence level and the spin up component of the third valence level couple to each other, causing level crossing near magnetic field $B=14$ T. Similarly, the fourth and fifth highest valence levels exhibit a level crossing near $B=14$ T.

To understand the origin of the valence levels in terms of bulk Bloch functions, we project the valence levels onto the Bloch functions of the heavy-hole, light-hole,

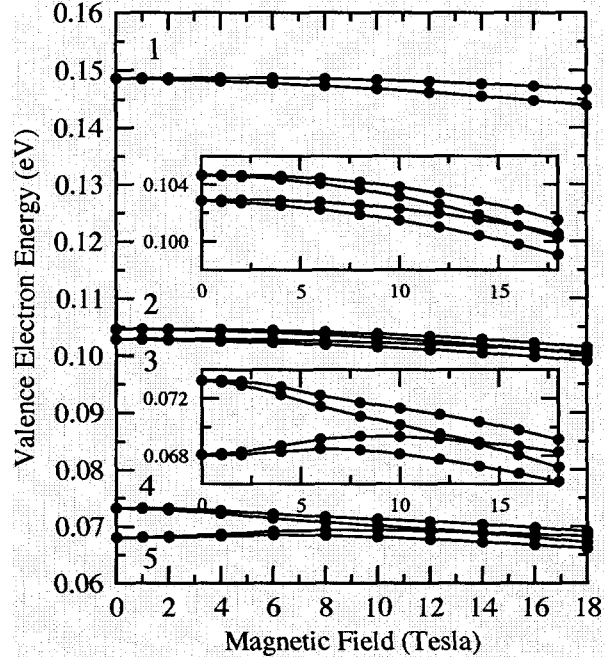


FIG. 2: Valence electron energies versus magnetic field along the growth direction of InAs self-assembled quantum dots. The two insets are a close-up of the evolution of the valence electron levels around 0.11 eV and 0.07 eV, respectively. Each valence level splits into two components due to a lifted spin degeneracy. For the valence levels around 0.11 eV and 0.07 eV, the Zeeman splitting between the spin up and down levels demonstrates a nonlinear response to the magnetic field. This nonlinearity results from the strong coupling between closely-spaced valence levels. The number near each line is the index for the valence level from the highest.

and split-off bands. The bulk Bloch functions are the eigenstates of the atomic total angular momentum \hat{j} and its z-component \hat{j}_z . With the notation of $|j, j_z\rangle$, the heavy-hole Bloch function is $|\frac{3}{2}, \pm\frac{3}{2}\rangle$, the light-hole $|\frac{3}{2}, \pm\frac{1}{2}\rangle$, and the split-off $|\frac{1}{2}, \pm\frac{1}{2}\rangle$. Therefore, the contributions of the bulk bands to a valence level $|\psi\rangle$ are given by $|\langle\frac{3}{2}, \frac{3}{2}|\psi\rangle|^2 + |\langle\frac{3}{2}, -\frac{3}{2}|\psi\rangle|^2$ for the heavy-hole band, $|\langle\frac{3}{2}, \frac{1}{2}|\psi\rangle|^2 + |\langle\frac{3}{2}, -\frac{1}{2}|\psi\rangle|^2$ for the light-hole band, and $|\langle\frac{1}{2}, \frac{1}{2}|\psi\rangle|^2 + |\langle\frac{1}{2}, -\frac{1}{2}|\psi\rangle|^2$ for the split-off band.

Figure 3 shows the bulk-band contributions to the first five highest valence levels. The heavy-hole band contributes the most, which is consistent with the bulk band structure at the Γ point. However, the light-hole and the split-off bands contribute as much as 20% and 5%, respectively. Therefore, the valence levels are not the eigenstates of \hat{j} and \hat{j}_z . The d band makes up 20% of the valence states, which is consistent with earlier results for bulk materials.^{16,17} The contributions of the s and s^* bands are negligible ($< 0.1\%$).

We investigate the magnetic-field effect on the transition rates between conduction $|\psi_c\rangle$ and valence $|\psi_v\rangle$ elec-

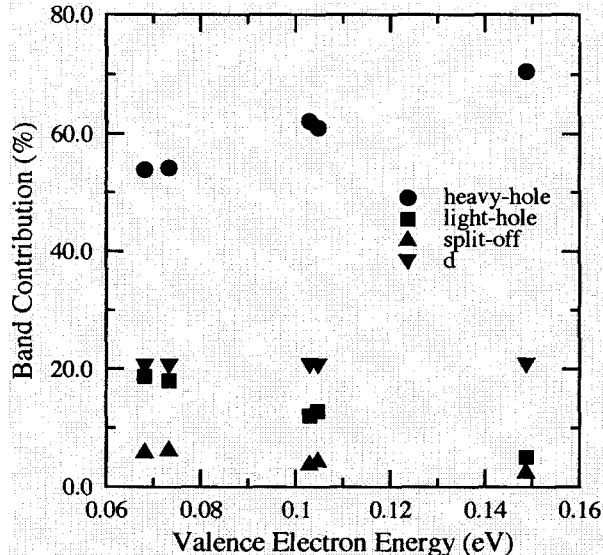


FIG. 3: Contributions of heavy-hole, light-hole, split-off, and d bands to valence electron states. As valence electron levels locate close to the bulk valence band edge (~ 0.22 eV), the contribution of the heavy-hole band increases while those of the light-hole and split-off bands decrease. The d band makes up about 20 % of all the valence electron states. There is a strong mixing between the heavy- and light-hole bands for valence electron states lower than the highest valence state.

tron levels when the self-assembled dot is excited with linearly polarized lights. The transition rate is given by

$$\Gamma(E) = \frac{2\pi}{\hbar} |\langle \psi_c | \hat{\mathbf{r}} | \psi_v \rangle|^2 \delta(E_c - E_v - E), \quad (1)$$

where E_c , E_v , and E are the energies of the conduction and valence electrons, and the excitation photon energy, respectively. The electron states are the linear combination of tight-binding orbitals $|i\gamma\rangle$, where i and γ are the indices for atomic site and orbital type, respectively. The dipole moment operator $\hat{\mathbf{r}}$ is decomposed into a discrete position vector operator $\hat{\mathbf{r}}_i$ of atomic site i and a relative position vector operator $\delta\hat{\mathbf{r}} = \hat{\mathbf{r}} - \hat{\mathbf{r}}_i$. With this decomposition, the dipole moment matrix element becomes²⁰

$$\langle \psi_c | \hat{\mathbf{r}} | \psi_v \rangle = \sum_{ii'\gamma\gamma'} c_{ci'}^* c_{vi\gamma} [\hat{\mathbf{r}}_i \delta_{ii'} \delta_{\gamma\gamma'} + \langle i'\gamma' | \delta\hat{\mathbf{r}}_i | i\gamma \rangle]. \quad (2)$$

The second part is the local dipole moment between tight-binding basis states. The real space description of the basis states is not known in empirical tight-binding model. As a reasonable guess, we choose Slater orbitals to represent the basis states.¹⁸ We further approximate the second part by including only the local dipole moments between the basis states on the same atomic site. The neglected off-site dipole moments are at least one order of magnitude smaller than the kept on-site dipole moments due to a small overlap between off-site orbitals.²⁰

TABLE I: Nonzero local dipole moments between tight-binding basis states for In, As, and Ga. The dipole moments are calculated by representing the basis states in real space with Slater orbitals (Ref. 18), and by using Monte Carlo integration (Ref. 19) for the radial parts and an exact integration for the angular parts. The symbols a and b denote two different cartesian-coordinate directions, for example x and y .

Dipole moment	In (Å)	As (Å)	Ga (Å)
$\langle s \hat{a} p_a \rangle$	1.106	0.754	0.961
$\langle s^* \hat{a} p_a \rangle$	0.196	0.123	0.167
$\langle p_a \hat{b} d_{ab} \rangle$	0.101	0.043	0.105
$\langle p_x \hat{x} d_{x^2-y^2} \rangle$	0.175	0.075	0.181
$\langle p_y \hat{y} d_{x^2-y^2} \rangle$	0.175	0.075	0.181
$\langle p_x \hat{x} d_{3z^2-r^2} \rangle$	0.058	0.025	0.061
$\langle p_y \hat{y} d_{3z^2-r^2} \rangle$	0.058	0.025	0.061
$\langle p_z \hat{z} d_{3z^2-r^2} \rangle$	0.116	0.049	0.121

The local dipole moments calculated with Slater orbitals are listed in Table I. Due to the selection rule of the local dipole moment operator $\delta\hat{\mathbf{r}}$, only the pairs of states with angular momentum difference $\delta\ell = 1$ yield nonzero dipole moments.

We obtain the absorption spectra of the quantum dots by summing the transition rates over the first four lowest conduction levels and the first five highest valence levels. To mimic thermal broadening, we broaden the delta function of the transition rate with a Gaussian function. The linewidth of the Gaussian function is chosen to be 50 meV which is comparable to that of experimental spectra.²¹

Figure 4 presents calculated absorption spectra of InAs self-assembled dots at magnetic fields 0 T, 10 T, and 18 T. As the magnetic field increases, the absorption peaks slightly shift and the peak near excitation energy 1.45 eV splits further. However, the relative heights of the absorption peaks remain unchanged. The first peak near energy 1.33 eV arises from $\langle \psi_c^1 | \hat{\mathbf{r}} | \psi_v^1 \rangle$, where $|\psi_c^n\rangle$ and $|\psi_v^n\rangle$ are the n -th lowest conduction and n -th highest valence levels, respectively. The second pronounced peak near 1.47 eV splits into two peaks in the presence of magnetic field. It results from $\langle \psi_c^2 | \hat{\mathbf{r}} | \psi_v^2 \rangle$ and $\langle \psi_c^2 | \hat{\mathbf{r}} | \psi_v^3 \rangle$. The third peak near 1.57 eV arises from $\langle \psi_c^3 | \hat{\mathbf{r}} | \psi_v^4 \rangle$ and $\langle \psi_c^3 | \hat{\mathbf{r}} | \psi_v^5 \rangle$, while the fourth peak near 1.58 eV from $\langle \psi_c^4 | \hat{\mathbf{r}} | \psi_v^4 \rangle$ and $\langle \psi_c^4 | \hat{\mathbf{r}} | \psi_v^5 \rangle$.

The origins of the absorption peaks illustrate that a given conduction level couples with only a couple of valence levels via the dipole moment operator. The selective dipole coupling can be explained by the symmetries of the electron levels. The dipole moment operator $\hat{\mathbf{r}}$ couples two levels with total angular momentum difference $\delta F = 1$, where $\hat{F} = \hat{L} + \hat{J}$. According to Eq. (2) for dipole-moment matrix elements, the selection rule $\delta F = 1$ is satisfied by two possible ways; (i) $\delta L = 1$ and $\delta J = 0$ or (ii) $\delta L = 0$ and $\delta J = 1$. Although the conduction and valence levels are not exactly the eigenstates of \hat{L} and \hat{J} , the expectation values of these operators are close to quantum

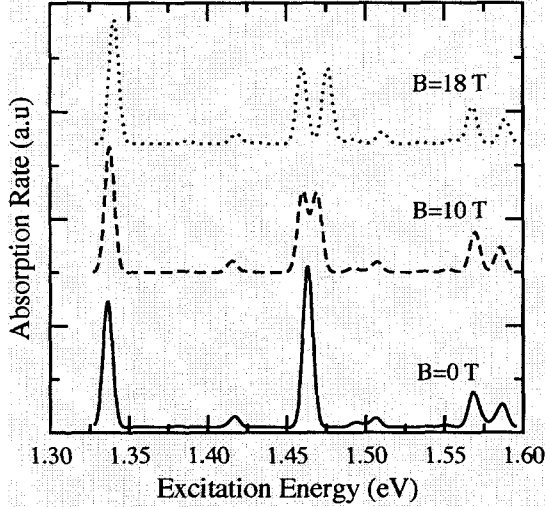


FIG. 4: Calculated absorption rate vs excitation energy. The absorption rate of InAs self-assembled quantum dot as a function of excitation energy is plotted for magnetic fields 0 T, 10 T, and 18 T. The magnetic field is oriented along the growth direction of the self-assembled dot. The excitation light is linearly polarized to the in-plane direction of the dot's substrate. The first 10 electron and hole levels are included in this calculation. Only a few absorption peaks are observed, indicating the existence of strong selection rules for electron-hole pair creation.

numbers. Therefore, we represent the electronic levels with the quantum number close to the expectation value. Within the notation of $|L, j\rangle$, the lowest conduction level is $|0, \frac{1}{2}\rangle$, and the highest valence level $|0, \frac{3}{2}\rangle$. Therefore, the transition $\langle\psi_c^1|\hat{x}|\psi_v^1\rangle$ satisfies the selection rule $\delta F = 1$ with $\delta L = 0$ and $\delta j = 1$. Similarly, the dipole transition between $|\psi_c^2\rangle = |1, \frac{1}{2}\rangle$ and $|\psi_v^{2,3}\rangle = |1, \frac{3}{2}\rangle$ is allowed. In

contrast, the transition between $|\psi_c^1\rangle$ and $|\psi_v^{2,3}\rangle$ and that between $|\psi_c^2\rangle$ and $|\psi_v^1\rangle$ are forbidden because $\delta L = 1$ and $\delta j = 1$.

The selective dipole coupling between conduction and valence levels remains intact even at high magnetic fields. Similar behavior is predicted for multishell nanocrystals by the $\mathbf{k} \cdot \mathbf{p}$ model.²² The robustness of the selection rule is attributed to the negligible magnetic coupling between levels with different quantum number L . Although there are magnetic couplings between valence levels (see insets of Fig. 2), the couplings are only between the levels with the same L . Since each level preserves its quantum number L at the variation of magnetic field, the selection rule for the dipole coupling between the levels remains the same. To observe the change in the selection rule, we estimate that the magnetic field needs to be as strong as 100 T. For a larger dot, the electron level spacing becomes smaller and therefore, the coupling between levels with different L can be observed at smaller magnetic fields.

In summary, we have investigated the magneto-optical response for InAs lens-shaped, self-assembled dots. The Zeeman splitting of conduction electron levels scales linearly with magnetic field, while that of valence levels shows a nonlinear response due to the strong coupling between closely-spaced levels. The transition rates between conduction and valence levels exhibit strong selection rules for electron-hole pair creations. This selective dipole coupling between levels remains intact even at a high magnetic field because the magnetic coupling between levels preserves the angular momentum L .

This work was carried out at Jet Propulsion Laboratory, California Institute of Technology, under a contract with the National Aeronautics and Space Administration. This work was supported by grants from NSA/ARDA, ONR, and JPL internal Research and Development.

- ¹ D. Loss and D. P. DiVincenzo, Phys. Rev. A **57**, 120 (1998).
- ² G. Burkard, D. Loss, and D. P. DiVincenzo, Phys. Rev. B **59**, 2070 (1999).
- ³ P. Recher, E. V. Sukhorukov, and D. Loss, Phys. Rev. Lett. **85**, 1962 (2000).
- ⁴ P. Keating, Phys. Rev. **145**, 637 (1966).
- ⁵ C. Pryor, J. Kim, L. W. Wang, A. J. Williamson, and A. Zunger, J. of Appl. Phys. **83**, 2548 (1998).
- ⁶ F. Oyafuso, G. Klimeck, P. von Allmen, T. B. Boykin, and R. C. Bowen, submitted to phys. stat. sol (2003).
- ⁷ T. B. Boykin, G. Klimeck, R. C. Bowen, and F. Oyafuso, Phys. Rev. B **66**, 125207 (2002).
- ⁸ P.-O. Löwdin, J. Chem. Phys. **18**, 365 (1950).
- ⁹ W. A. Harrison, *Elementary Electronic Structure* (World Scientific, New Jersey, 1999).
- ¹⁰ J. C. Slater and G. F. Koster, Phys. Rev. **94**, 1498 (1954).
- ¹¹ D. J. Chadi, Phys. Rev. B **16**, 790 (1977).
- ¹² R. Peierls, Z. Phys. **80**, 763 (1933).
- ¹³ M. Graf and P. Vogl, Phys. Rev. B **51**, 4940 (1995).
- ¹⁴ T. B. Boykin, R. C. Bowen, and G. Klimeck, Phys. Rev. B **63**, 245314 (1995).
- ¹⁵ <http://www.caam.rice.edu/software/ARPACK/>.
- ¹⁶ P. Boguslawski and I. Gorczyca, Semicond. Sci. Technol. **9**, 2169 (1994).
- ¹⁷ J.-M. Jancu, R. Scholz, F. Beltram, and F. Bassani, Phys. Rev. B **57**, 6493 (1998).
- ¹⁸ J. C. Slater, Phys. Rev. **36**, 57 (1930).
- ¹⁹ W. H. Press, S. A. Teukolsky, W. T. Vetterling, and B. P. Flannery, *Numerical Recipes in C: The Art of Scientific Computing* (Cambridge University Press, 1999), 2nd ed.
- ²⁰ S. Lee, J. Kim, L. Jönsson, J. W. Wilkins, G. W. Bryant, and G. Klimeck, Phys. Rev. B **66**, 235307 (2002).
- ²¹ P. P. Paskov, P. O. Holtz, B. Monemar, J. M. Garcia, W. V. Schoenfeld, and P. M. Petroff, Phys. Rev. B **62**, 7344 (2000).
- ²² J. Planelles, J. Climente, J. G. Díaz, and W. Jaskólski, J. Phys.: Condens. Matter **14**, 12537 (2002).